



Combustion behavior profiling of single pulverized coal particles in a drop tube furnace through high-speed imaging and image analysis



Xiaojing Bai^{a,b}, Gang Lu^{b,*}, Tom Bennet^c, Archi Sarroza^c, Carol Eastwick^c, Hao Liu^{c,*}, Yong Yan^b

^aSchool of Control and Computer Engineering, North China Electric Power University, Beijing 102206, China

^bSchool of Engineering and Digital Arts, University of Kent, Canterbury, Kent CT2 7NT, UK

^cFaculty of Engineering, University of Nottingham, University Park, Nottingham NG7 2RD, UK

ARTICLE INFO

Article history:

Received 20 September 2016

Received in revised form 24 February 2017

Accepted 12 March 2017

Available online 14 March 2017

Keywords:

Pulverized coal particles

Drop tube furnace

High-speed imaging

Image processing

Combustion behaviors

ABSTRACT

Experimental investigations into the combustion behaviors of single pulverized coal particles are carried out based on high-speed imaging and image processing techniques. A high-speed video camera is employed to acquire the images of coal particles during their residence time in a visual drop tube furnace. Computer algorithms are developed to determine the characteristic parameters of the particles from the images extracted from the videos obtained. The parameters are used to quantify the combustion behaviors of the burning particle in terms of its size, shape, surface roughness, rotation frequency and luminosity. Two sets of samples of the same coal with different particle sizes are studied using the techniques developed. Experimental results show that the coal with different particle sizes exhibits distinctly different combustion behaviors. In particular, for the large coal particle (150–212 μm), the combustion of volatiles and char takes place sequentially with clear fragmentation at the early stage of the char combustion. For the small coal particle (106–150 μm), however, the combustion of volatiles and char occurs simultaneously with no clear fragmentation. The size of the two burning particles shows a decreasing trend with periodic variation attributed to the rapid rotations of the particles. The small particle rotates at a frequency of around 30 Hz, in comparison to 20 Hz for the large particle due to a greater combustion rate. The luminous intensity of the large particle shows two peaks, which is attributed to the sequential combustion of volatiles and char. The luminous intensity of the small particle illustrates a monotonously decreasing trend, suggesting again a simultaneous devolatilization/volatile and char combustion.

© 2017 The Authors. Published by Elsevier Inc. This is an open access article under the CC BY license (<http://creativecommons.org/licenses/by/4.0/>).

1. Introduction

Although renewable energy has been attracting much attention in recent years due to environmental concerns, conventional fuels such as pulverized coal will remain a major worldwide energy resource for years to come due to their wide availability and competitively low cost, particularly with the development of new combustion technologies such as co-firing coal and biomass and oxy-coal combustion [1]. While the effects of chemical composition and other fuel properties of coal on combustion have been widely studied, the physical characteristics of a pulverized solid fuel, such as particle size, and shape have also been found to have a significant impact on the ignition and combustion behaviors of fuel particles, and consequently the flame stability, combustion efficiency

and pollutant emissions [2]. The combustion process of solid fuel particles comprises typically three stages, i.e., heating, volatilization/devolatilization, and char oxidization [3]. Depending upon not only the fuel properties, but also the heating rate, particle size, combustion environments (temperature and stoichiometry, etc.) and the volatile matter evolution, the homogeneous ignition and heterogeneous ignition of fuel particles may occur sequentially or simultaneously [4]. This makes it more difficult to characterize the combustion behaviors of fuel particles. Therefore, the measurement and characterization of individual fuel particles are required to explore the insight into the combustion mechanism of fuel particles, and consequently advance the knowledge to optimize combustion processes and validate computational modeling results.

There is a range of experimental and modeling work that has been carried out to investigate the combustion behaviors of coal and biomass fuel particles of different ranks and sizes under different combustion conditions in drop tube furnaces (DTFs), using non-visualized and visualized technical approaches [5–11]. For instance, Wang et al. [12] investigated the combustion behaviors and ash characteristics of coal and biomass particles through analyzing

* Corresponding authors.

E-mail addresses: xb9@kent.ac.uk (X. Bai), g.lu@kent.ac.uk (G. Lu), tombennet@gmail.com (T. Bennet), acsarroza@hotmail.co.uk (A. Sarroza), carol.eastwick@nottingham.ac.uk (C. Eastwick), liu.hao@nottingham.ac.uk (H. Liu), y.yan@kent.ac.uk (Y. Yan).

the particles sampled from different heights of the DTF, using X-ray fluorescence spectroscopy and a particle size analyzer. Costa et al. [13] evaluated the gas temperature, particle burnout and particle fragmentation of raw and torrefied pine shells and olive stones in a DTF using various instruments (e.g. a low pressure three-stage cascade impactor, a particle size analyzer and a scanning electron microscope). Pereira et al. [14] studied the kinetics of poplar short rotation coppice in a DTF through thermogravimetric analysis. The above investigations are based on non-visualized technical approaches. With the advent of high-speed digital imaging and image processing techniques, the visualization and characteristics of burning particles have become feasible. Simões et al. [11] investigated the ignition mode and delay time of biomass fuels through the analysis of particle images from a high-speed camera. The impact of gas temperature and oxygen concentration on the ignition mode and ignition delay time was assessed. Shaddix and Molina [15] analyzed the ignition and devolatilization characteristics of both high-volatile bituminous and subbituminous coal particles through single-particle imaging in both N_2 and CO_2 diluent gasses. Kim et al. [16] investigated the ignition behaviors of coal particles under high heating-rate conditions using a flat flame burner and particle images. Levendis et al. [4,17] and Rianza et al. [1] employed three-color pyrometry and high-speed high-resolution cinematography to study the combustion behaviors of single coal particles in both air and simulated oxy-fuel environments. Köser et al. [18] also studied the combustion characteristics of individual coal particles in an oxygen-enriched environment using high-speed OH-PLIF (Planar Laser-induced Fluorescence).

Although certain progress on the characterization of burning particles using visualized approaches has been made, few studies have been undertaken on the quantitative profiling of single fuel particles. Podczek [19] proposed a shape factor, which used the deviations of the 2-D (two-dimensional) particle outlines from the images of a circle, triangle and square, for the particle analysis. Gao et al. [20] conducted the on-line measurement of particle size and shape and their distributions through image processing, where the images of particles were acquired from a color CCD camera coupled with multi-wavelength laser sources. Carter et al. [21] and Qian et al. [22] combined digital imaging and electrostatic sensors to obtain the size distribution and volumetric concentration of particles in pneumatic conveying pipes. It is clear that, while the combustion behaviors of fuel particles influence the overall performance of a combustion process, limited studies have been carried out to investigate the combustion behaviors of burning particles through the measurement of physical characteristics such as size, shape, surface roughness, rotational frequency and luminosity.

This paper presents experimental investigations into the combustion behaviors of individual coal particles with the aim of providing a quantitative description of particle dynamics during combustion through high-speed imaging and digital image processing. The videos of two sets of individual coal particles were recorded using a high-speed camera during the combustion process in a visual drop tube furnace (V-DTF). Algorithms are developed to acquire and process the particle images in terms of physical quantities, including size, shape, surface roughness, rotation and luminosity. These quantities are then used to describe the characteristics of the burning particles during their residence time in the furnace.

2. Materials and methods

2.1. V-DTF and high-speed camera

DTFs have been widely used for combustion research as they can provide critical data for the in-depth understanding of ignition

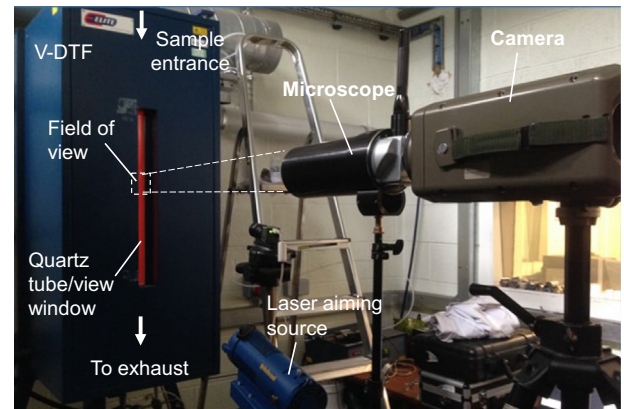


Fig. 1. Overview of the experimental setup.

and combustion behaviors of fuel particles in power plant boilers [23]. The tiny size, short residence time of the particles and the variations of the size and shape make it very difficult to visualize and characterize the burning particles. With the aid of high-speed imaging, it is possible to visualize burning particles in a DTF. Fig. 1 is the overview of the experimental setup in this study. The V-DTF used in this study is an electrically heated drop tube furnace equipped with a 1400 mm long quartz tube with an inner diameter of 50 mm, capable of maintaining gas temperatures up to 1050 °C within the 1000 mm-long heated zone [24,25]. The quartz work tube is insulated by a spun ceramic fiber blanket to minimize the heat loss during experimentation. The fuel particles are injected into the quartz tube from the water-cooled feed probe mounted at the top of the quartz tube. The particles are heated, ignited and combusted in the furnace with the residual ash being vacuumed away or collected with the collection probe mounted at the bottom end of the quartz tube. There is a long and narrow viewing window at the front side of the furnace which allows a camera system to access and view the combustion process of the fuel particles inside the quartz tube.

A high-speed camera (Phantom v12.1), capable of recording a video at a frame rate up to 1,000,000 fps (frames per second), acquires videos of burning coal particles. A long-distance microscope (Qestar QM-1, which has a 56–152 cm working distance, a 30–1 variability in the field of view and a resolution better than 3 μm at 56 cm) is coupled with the camera to ensure that coal particles can be captured during their residence time in the furnace. The resulting field of view is around 8 mm \times 8 mm.

2.2. Coal properties and test conditions

Two sets of coal sample with different particle sizes (Particles A and B) were prepared from the same batch of Colombian bituminous coal (El Cerrejon, which was sourced directly from a UK power plant). Each sample was separately dried, sieved with particle size ranging from 150 to 212 μm for Particle A, and 106 to 150 μm for Particle B. The proximate and ultimate analyses of the samples are summarized in Table 1. In the test, a small amount (in milligrams) of the sieved coal particles were dropped manually through the feed probe into the quartz tube which was pre-heated to 800 °C and supplied with air at a rate of 5 L/min. The high-speed camera tracked and took the videos of the particles at a frame rate of 6200 fps during their residence time in the quartz tube.

2.3. Contour detection and extraction

Once the videos were recorded, individual images of a particle were read frame by frame in a computer. Image progressing algo-

Table 1
Proximate and ultimate analyses^a of El Cerrejon.

Proximate analysis (% as received)		Ultimate analysis (% dry basis)	
Moisture	2.3	Carbon	72.2
Volatile matter	36.6	Hydrogen	4.8
Fixed carbon	51.4	Oxygen	9.1
Ash	9.7	Nitrogen	1.5
		Sulphur	2.4
High heating value: MJ/kg (dry basis)		29.6	

^a BS ISO 17246:2010 and BS ISO 17247:2013.

gorithms were then developed to process the images. Detecting the particle contour is the initial step in the image processing. Otsu's method [26] was used to automatically segment the images. Otsu's method calculates the optimum threshold separating the histogram of an image into two pixel groups (i.e., foreground and background groups) and ensures that the intra-class variance is minimal or equivalent. Once the threshold is determined, the binary format of the image is generated, which allows the particle contour retrieval to be performed. The 8-connectivity, which traces neighbors to every pixel that touches one of their edges [20], is then used to extract the contour of the particle's binary image. These pixels are connected horizontally, vertically, and diagonally. The 8-connectivity can be described as,

$$\max(|x' - x''|, |y' - y''|) = 1, \quad (1)$$

where (x', y') and (x'', y'') are a pair of pixels in the image. Once the particle contour is determined, a set of characteristic parameters, which describe the particle size, shape, surface roughness, rotation and luminosity, are computed.

2.4. Characteristic parameters

2.4.1. Size and shape

Two parameters, i.e., *Area* and *Aspect ratio*, are defined to describe the size and shape of the particle.

Area (A) – The Area is the quantity representing the particle size. A is determined by counting the pixel number within the particle contour, R , i.e.,

$$A = \sum_{(i,j) \in R} 1. \quad (2)$$

Aspect ratio (R_a) – The Aspect ratio is the ratio of the major axis to the minor axis of the equivalent ellipse of a particle [27], and is calculated as,

$$R_a = \frac{L}{W}, \quad (3)$$

where L and W are the lengths of the major and minor axes, respectively, as shown in Fig. 2. For a circle, R_a is 1. The larger the R_a , the more elongated the particle.

2.4.2. Surface roughness

Two parameters, *Boundary distance* and *Boundary variance index*, are computed for quantifying the surface roughness of the particle.

Boundary distance [$r(k)$] – The Boundary distance is the distance between a point (x_k, y_k) on the boundary and the center (x_c, y_c) of the particle, i.e.,

$$r(k) = \sqrt{(x_k - x_c)^2 + (y_k - y_c)^2}, \quad (4)$$

where, $k = 0, 1, 2, \dots, N - 1$, N is the number of the boundary points, and, in this study, $N = 128$.

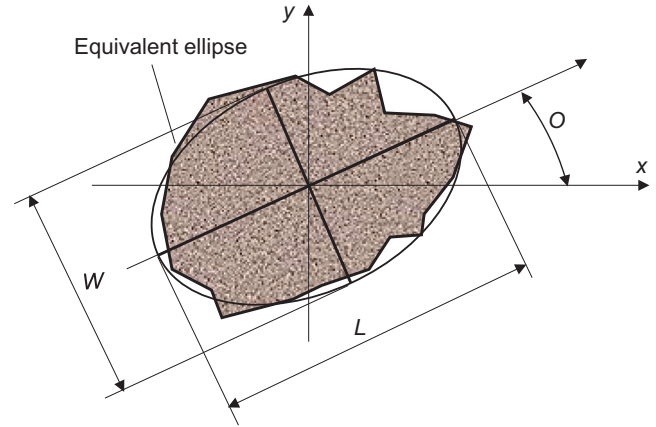


Fig. 2. A particle and its equivalent ellipse.

By using (4), the boundary of the particle is transformed into a one-dimensional 'signal' in the spatial domain and thus the discrete Fourier transform (DFT) is performed over $r(k)$ [28], i.e.,

$$F(n) = \frac{1}{N} \sum_{k=0}^{N-1} r(k) e^{-j2\pi nk/N}, \quad (5)$$

where $n = 0, 1, 2, \dots, N - 1$. Once the DFT form of the boundary distance is obtained, the variance of the boundary is determined.

Boundary variance index – The Boundary variance index, $DF = [DF_1, DF_2, \dots, DF_{N/2}]$, is the ratio of the absolute values of $F(n)$ ($n = 1, 2, \dots, N/2$) to the absolute value of the DC (Direct Current) component $|F(0)|$, i.e.,

$$DF_n = \frac{|F(n)|}{|F(0)|}, \quad (6)$$

where $|F(0)|$ is the average of the boundary distance [29]. The variance of the DF represents the variance of the boundary in different scales. The rougher the boundary, the greater the DF .

2.4.3. Rotation

Previous studies revealed that coal particles rotate rapidly during combustion due to volatile releases and/or the intensive exothermic combustion reactions [30]. The rotation of a particle can be quantified through the computation of the change in particle orientation during its residence time in the furnace. High-speed imaging has made it possible to derive parameters relating to the motion of the particles such as orientation and rotational frequency. The orientation, O , is counted as the angle between the major axis and the x-axis of the equivalent ellipse of the particle, i.e. [31],

$$O = \arctan \left(\frac{|\sum_{i \in R} x_i^2 - \sum_{i \in R} y_i^2| + \sqrt{(\sum_{i \in R} x_i^2 - \sum_{i \in R} y_i^2)^2 + 4(\sum_i x_i y_i)^2}}{2 \sum_i x_i y_i} \right), \quad (7)$$

where (x_i, y_i) are the coordinates of pixel i within the equivalent ellipse. Rotation index of the particle, R_{ind} , is then defined as,

$$R_{ind} = \pm \sin(O). \quad (8)$$

R_{ind} ranges from -1 to 1 , where $R_{ind} = 1$ stands for 90° and $R_{ind} = -1$ stands for 270° . Note that the sign is dependent upon the orientation of the particle computed from the former image frame and the initial sign is defined as positive.

2.4.4. Luminosity

The luminous intensity of a burning coal particle is highly related to its surface temperature [21]. In general, a higher luminous intensity entails a higher surface temperature [7]. The normalized luminous intensity, G , is the averaged grey-level intensity of the particle image normalized to the maximum grey-level of the image (255 in this study), i.e.,

$$G = \frac{\sum_{(i,j) \in K} I_{ij}}{255A} \times 100\%, \tag{9}$$

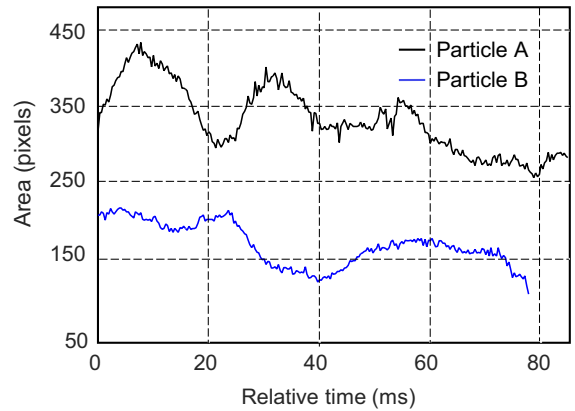
where I_{ij} is the grey-level of the image at pixel (i, j) and A is the area defined in (2).

3. Experimental results

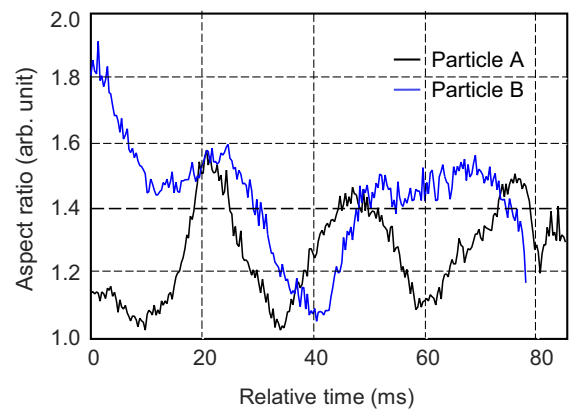
Fig. 3 shows the example images of the coal particles captured by the camera system. The sample images provide visualized information associated with the combustion behaviors of the two particles. It should be noted that, by the time when the particle was captured by the camera, it had been in the quartz tube for some time, and thus each image frame does not represent the absolute residence time of the particle in the quartz tube, but the relative residence time between frames, e.g., two successive frames represent a relative residence time of 0.2 ms. The combustion of volatiles and char including fragmentation of the particles were clearly observed from the images. As expected, the combustion behaviors of the particles varied significantly in their residence time. The quantification of such variations was performed in terms of the characteristic parameters defined in Section 2.

3.1. Size and shape characteristics

Fig. 4(a) shows the area variation of the coal particles during their residence time in the quartz tube. A decreasing trend is evident for both Particles A and B due to the mass loss of the

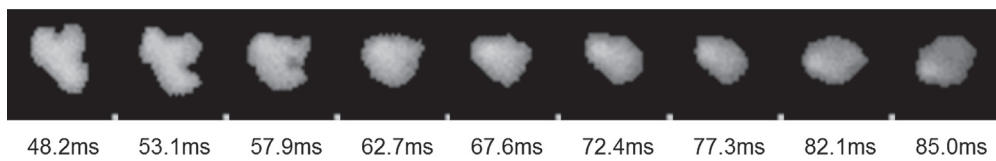
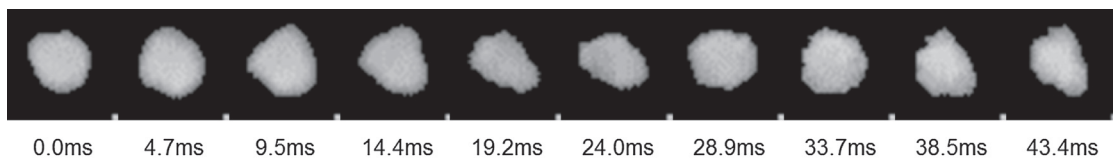


(a) Area.

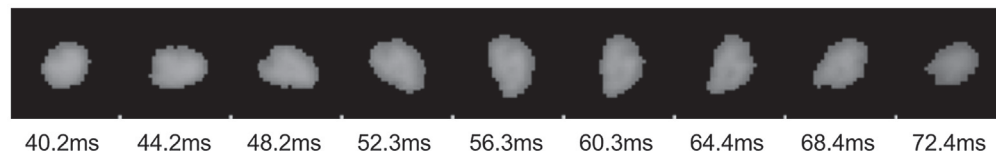
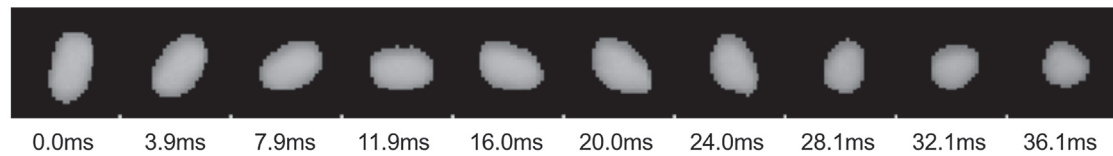


(b) Aspect ratio.

Fig. 4. Variation of the area and aspect ratio of the coal particles.



(a) Particle A (150–212 μm).



(b) Particle B (106–150 μm).

Fig. 3. Example images of coal particles by frames and relative time.

particles during combustion. The periodic variation of the particle area is believed to be due to the rotation of the particle in the line-of-sight direction of the camera system. It is also observed that the combustion behaviors of the two particles differ due to their different sizes. For instance, for Particle A, the devolatilization/volatile combustion dominated before about 20 ms. It is evident that the boundaries of the particle were clear and smooth [refer to Fig. 3(a), and also the later section about

the surface roughness]. It is observed in the video [refer to Fig. 3(a)] that the fragmentation of the particle started from about 20 ms, and the significant char combustion began around 40 ms. These are also evident in Fig. 4(a) and (b) where the area and shape of the particle show great fluctuations in the period from 20 to 40 ms. The single-phase char combustion began around 60 ms [refer to Fig. 3(a)], toward to the completion of combustion. For Particle B, as it is relatively small in size

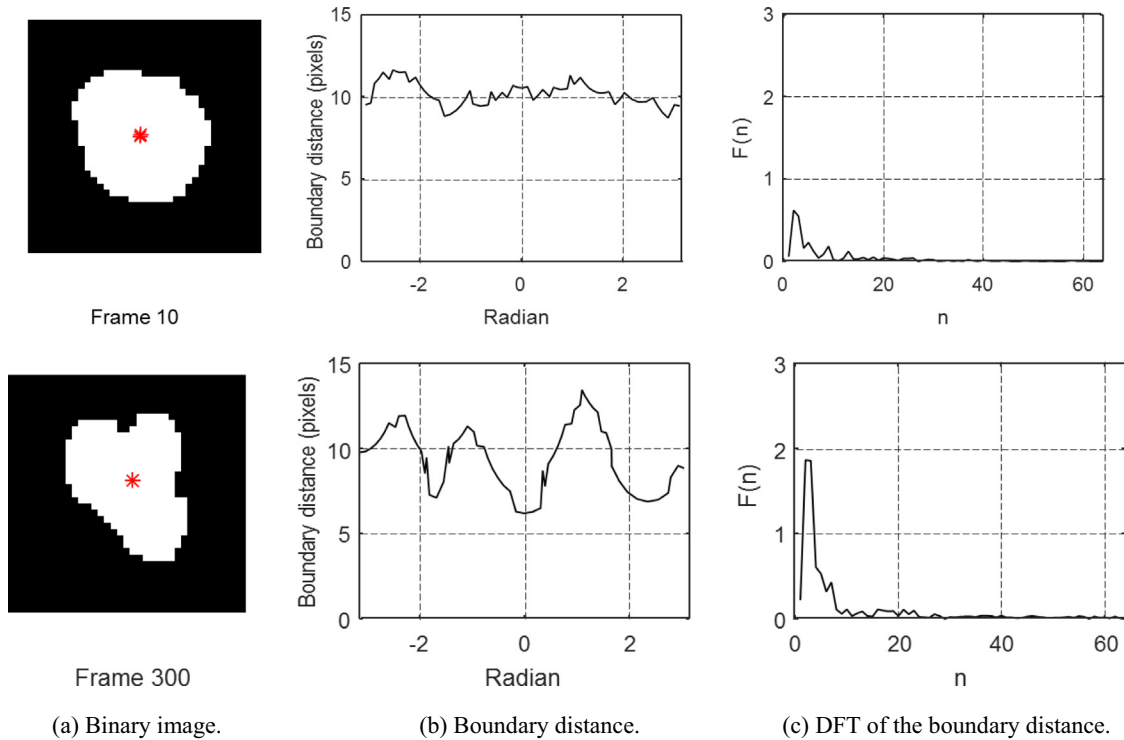


Fig. 5. Binary image, boundary distance and DFT of Particle A for Frames 10 (at 1.5 ms) and 300 (at 48.4 ms).

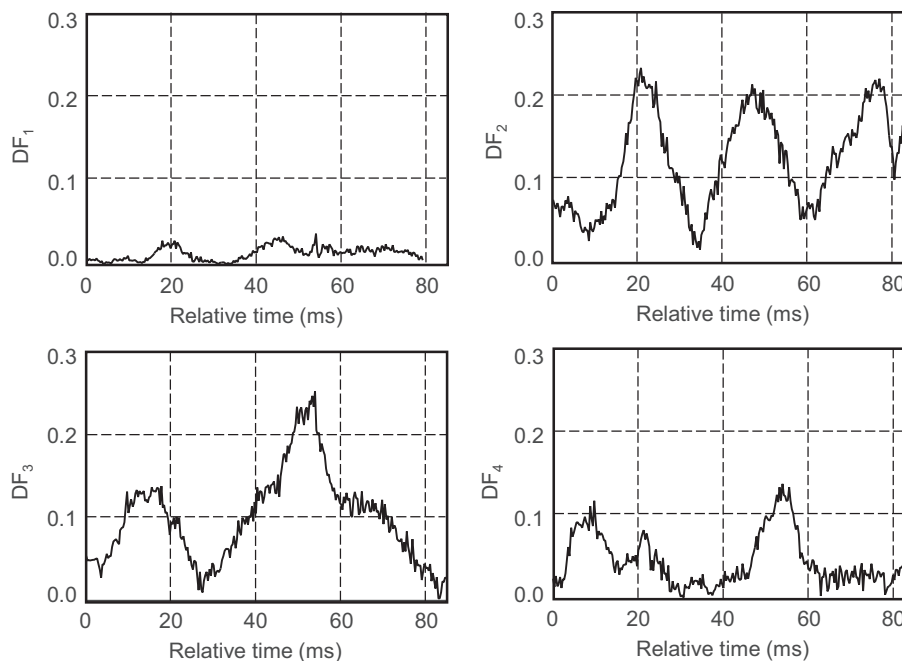


Fig. 6. Boundary variance index of boundary distance of Particle A.

(106–150 μm), the combustion of volatiles and char appeared to take place simultaneously at the initial stage of combustion, and fragmentation was not visualized. This is supported by the fact that the particle area decreased gradually during the initial stage of combustion process (0–24 ms), which is believed to be the result of the simultaneous combustion of volatiles and char. The single-phase char combustion appeared to begin around 24 ms [refer to Fig. 3(b)].

Fig. 4(b) suggests that the aspect ratio of Particle A ranges between 1.0 and 1.6 but the averaged value tends to be greater in its residence time, suggesting that the shape of the particle changed from ‘round’ to ‘longitudinal’ during combustion. A periodic variation is also clearly seen with a period of around 25 ms (163 frames), which is similar to the period of the area variation [Fig. 4(a)], which is again believed to be due to the particle rotation in the line-of-sight direction. On the other hand, the aspect ratio of Particle B varies from 1.0 to 1.8, suggesting that Particle B is slightly ‘longer’ than Particle A. A decreasing trend is also found, indicating that the shape of particle changed from ‘longitudinal’ to ‘round’ during its residence time.

With regard to the surface roughness of the particles, Fig. 5 shows two typical examples of the binary images of Particle A, i.e., Frame 10 (at 1.5 ms) and Frame 300 (at 48.4 ms), and the corresponding boundary distance $r(k)$, and the DFT of $r(k)$. As can be seen, the profile of the boundary distances differs significantly from one frame to another. Compared to the frequency of Frame 300, there are fewer low-frequency components of Frame 10 due to the fact that the boundary of Frame 10 is smoother than that of Frame 300 [Fig. 5(a)]. As the difference in surface roughness is mainly shown in the low frequency band, only the first four components, DF_1 – DF_4 , are further analyzed.

Fig. 6 presents DF_1 – DF_4 of the boundary variance index for Particle A. It reveals that DF_1 , which represents the lowest frequency variance among the four components, is lower than the other three components. DF_2 shows a periodical trend which is considered to be related to the rotation of the particle. It was observed in the video that there were some fragments broken up from the main

particle during the later stage of devolatilization/volatile combustion and the initial stage of char combustion, i.e., between 20 ms and 60 ms. The results illuminate that the fragmentation and char combustion of the coal particle affect the boundary variance in different scales, especially at higher frequency components, i.e., DF_3 and DF_4 .

Fig. 7 illustrates DF_1 – DF_4 of the boundary variance index for Particle B. Similar to Particle A, DF_1 is lower than the other three. DF_2 has the lowest value at around 40 ms, indicating a smoother surface of Particle B at that period of time. In addition, DF_1 – DF_3 vary irregularly but have much lower amplitudes in comparison to that of Particle A, suggesting that Particle B has a smoother surface than Particle A. This may be attributed to the fact that Particle B has no obvious fragmentation during combustion as a result of its smaller size in comparison to Particle A. The results have also suggested that the particle fragmentation and char combustion are the main contributors to the surface roughness of the particles.

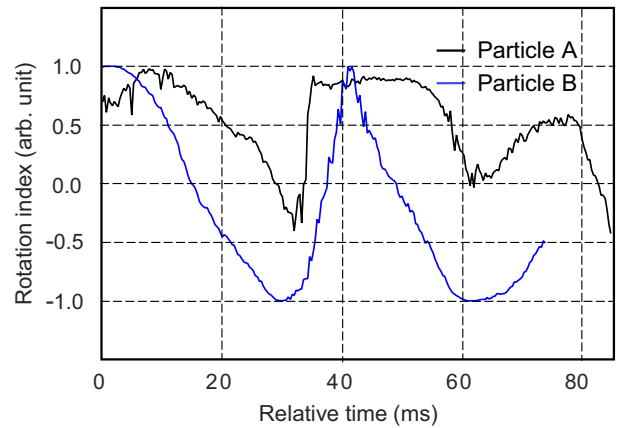


Fig. 8. Rotation index of the coal particles.

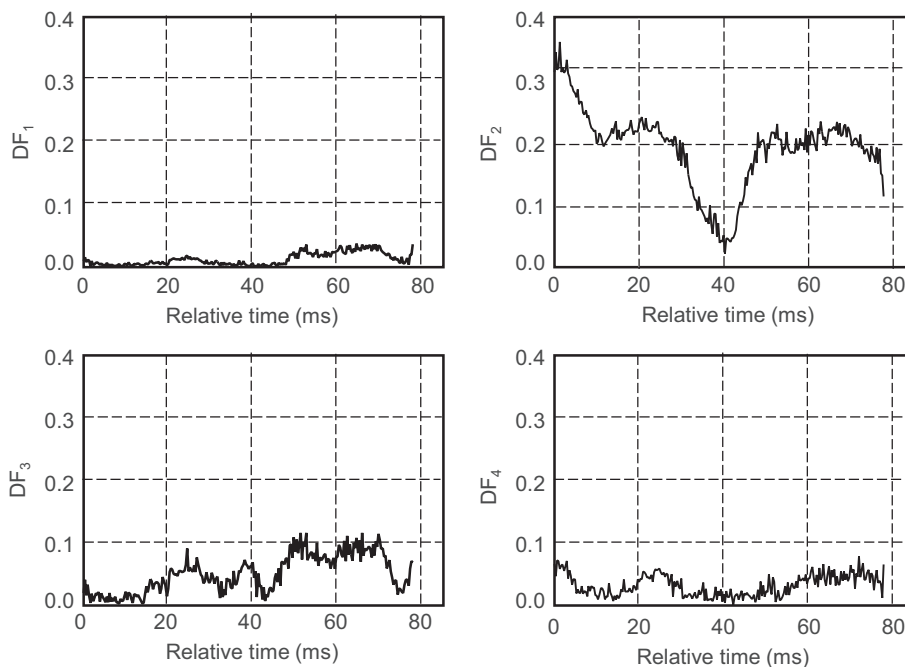


Fig. 7. Boundary variance index of boundary distance of Particle B.

3.2. Rotational characteristics

The rotation variance of the particle is owing to the momentum changes caused by the heterogeneous combustion. Fig. 8 shows that the rotation index of Particle A has a similar periodic variation as observed in Fig. 4. Again, the periodic variation is believed to be attributed to the rotation of the particle in the line-of-sight of the camera system. It is also noted that the rotation index of Particle A varies in a range between -0.25 and 1 (i.e., 90° and 200°), which does not mean that the particle does not rotate but may be attributed to the case that the rotation direction of the particle is close to the line-of-sight. It can be found in Fig. 4 that the period of the area variation of Particle A is around 50 ms (computed between the two peaks), suggesting a rotational frequency of 20 Hz. In contrast, the period of the area variation of Particle B is 33 ms, which means the rotational frequency of Particle B is around 30 Hz. The higher rotational frequency of Particle B may be attributed to the smaller size (hence a greater influence of the gaseous flow in the DTF), greater combustion rate and no fragmentation (which would reduce the motion of the particle) in comparison to Particle A.

3.3. Luminous characteristics

As mentioned earlier, the luminous intensity of the burning particles in the images is closely related to the surface temperature of the particles. It is believed that, in general, the higher the luminous intensity, the higher the surface temperature and thus more intensive combustion reactions. Fig. 9 exhibits the pseudo color images of the luminous intensity of the burning particles. It is found that the luminosity of both particles is relatively homogeneous during the early stage of the combustion, which is because of the volatile combustion in that period of time. When the volatile combustion is about to finish, however, the luminosity becomes heterogeneous due to the inhomogeneous char combustion as a result of ash layer formed in the remaining char particle. The variations of the

luminous intensity of the particles can be more clearly seen in Fig. 10. The normalized luminous intensity of Particle A shows a periodical trend from 0 ms to about 40 ms, and then a decreasing trend, indicating that its luminous intensity decreases toward the later stage (at around 20 ms) of the devolatilization/volatile combustion and increase with the initial stage of char combustion (the significant char combustion of the core particle started around 40 ms). A decreasing rate of $0.58\%/ms$ is found from 42 ms to 83 ms, suggesting the significant consumption of carbon in the remaining char particle. In contrast, a monotonous decreasing trend is observed from the normalized luminous intensity of Particle B (Fig. 10). This indicates that the combustion of volatiles and char took place at the same time from the beginning (when the particle's burning can be picked up by the camera) and hence a heterogeneous combustion all the way. It is also noted that the luminous intensity decreased dramatically after 75 ms, indicating the completion of the combustion.

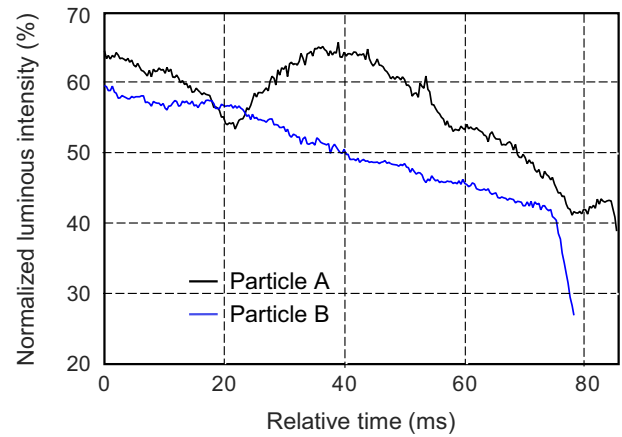


Fig. 10. Normalized luminous intensity of the coal particles.

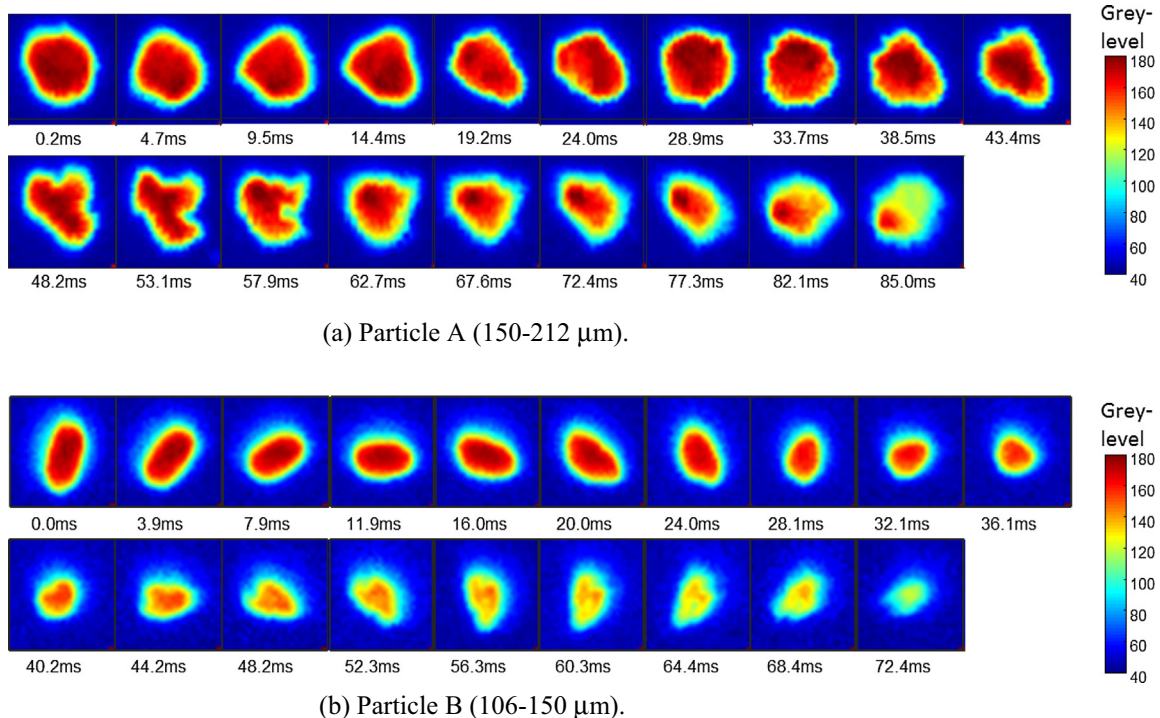


Fig. 9. Pseudo color images of the luminous intensity of the particles.

It should be mentioned that the experimental results presented above have suffered from uncertainties in some extent. The uncertainty of the measurement can be attributed to the image resolution, especially considering the tiny size of coal particles. The boundary of the particle in the images can be irregular and sometimes blur, which can result in a low signal-to-noise ratio, and thus an uncertainty in the calculation of the physical parameters. In the presented study, the particle sizes range from 106 μm to 212 μm , which gave us reasonable image sizes, and thus the uncertainty caused would not introduce a significant error in the calculation. In addition, the particles are of 3-D arbitrary shape, but the computed parameters are based on their 2-D images. This also introduces an uncertainty, which is unavoidable and difficult to assess. From a statistic analysis point of view, however, such an uncertainty would not make a significant impact on the results.

4. Conclusions

In this study, the combustion behaviors of two sets of coal particles with different sizes have been investigated using high-speed imaging and image processing techniques. Characteristic parameters including area, aspect ratio, boundary distance, boundary variance index, rotation index and normalized luminous intensity have been defined and computed to quantify the combustion behaviors of the particles. It has been found that the coal with different particle sizes and shapes exhibits distinctly different combustion behaviors. For the large coal particle, the combustion of volatiles and char takes place sequentially, while, for the small particle, the combustion of volatiles and char occurs at the same time. The results have also shown that the size of the particles has a decreasing trend due to the combustion of volatiles and char with periodic variations which is attributed to the rotation of the particles. The fragmentation and char combustion have caused significant changes in the surface roughness of the particles. In addition, the luminosity of the large particle shows two peaks when the combustion of volatiles and char happen sequentially, while the luminosity of the small particle decreases monotonously when the combustion of volatile and char occurs simultaneously. It can be concluded that the combination of high-speed imaging and image processing has provided a feasible and effective means for characterizing the combustion behaviors of burning coal particles. Further applications of the developed techniques will be extended to the study of combustion behaviors of pulverized biomass and biomass/coal blends under various combustion conditions.

Acknowledgements

This work was supported by the UK Engineering and Physical Sciences Research Council [grant number: EP/G037345/1], the UK Carbon Capture and Storage Research Centre [EP/K000446/1, EP/K000446/2, Call 1 Project: C1-27], Doosan Babcock Ltd., Scottish and Southern plc. (SSE), and the 111 Talent Introduction Project [B13009] at North China Electric Power University of the Chinese Ministry of Education. Dr Yizhen Peng in the School of Information Engineering, Tianjin University of Science and Technology, China is also acknowledged for his contribution to this study. The China Scholarship Council is acknowledged for providing a fellowship to Xiaojing Bai for studying at the University of Kent.

References

- [1] J. Riaza, R. Khatami, Y.A. Leventdis, L. Álvarez, M.V. Gil, C. Pevida, F. Rubiera, J.J. Pis, Single particle ignition and combustion of anthracite, semi-anthracite and bituminous coals in air and simulated oxy-fuel conditions, *Combust. Flame* 161 (2014) 1096–1108, <http://dx.doi.org/10.1016/j.combustflame.2013.10.004>.
- [2] M. Momeni, C. Yin, S.K. Kær, T.B. Hansen, P.A. Jensen, P. Glarborg, Experimental study on effects of particle shape and operating conditions on combustion characteristics of single biomass particles, *Energy Fuels* 27 (2012) 507–514, <http://dx.doi.org/10.1021/ef301343q>.
- [3] Z. Wu, *Fundamentals of pulverised coal combustion*, in: IEA Clean Coal Centre Reports, London, UK, IEA Clean Coal Centre, 2005, p. 36.
- [4] Y.A. Leventdis, K. Joshi, R. Khatami, A.F. Sarofim, Combustion behavior in air of single particles from three different coal ranks and from sugarcane bagasse, *Combust. Flame* 158 (2011) 452–465, <http://dx.doi.org/10.1016/j.combustflame.2010.09.007>.
- [5] C. Zou, L. Cai, D. Wu, Y. Liu, S. Liu, C. Zheng, Ignition behaviors of pulverized coal particles in O_2/N_2 and $\text{O}_2/\text{H}_2\text{O}$ mixtures in a drop tube furnace using flame monitoring techniques, *Proc. Combust. Inst.* 35 (2015) 3629–3636, <http://dx.doi.org/10.1016/j.proci.2014.06.067>.
- [6] G. Wang, R. Zander, M. Costa, Oxy-fuel combustion characteristics of pulverized-coal in a drop tube furnace, *Fuel* 115 (2014) 452–460, <http://dx.doi.org/10.1016/j.fuel.2013.07.063>.
- [7] H. Lee, S. Choi, An observation of combustion behavior of a single coal particle entrained into hot gas flow, *Combust. Flame* 162 (2015) 2610–2620, <http://dx.doi.org/10.1016/j.combustflame.2015.03.010>.
- [8] P.E. Mason, L.I. Darvell, J.M. Jones, M. Pourkashanian, A. Williams, Single particle flame-combustion studies on solid biomass fuels, *Fuel* 151 (2015) 21–30, <http://dx.doi.org/10.1016/j.fuel.2014.11.088>.
- [9] P. Escot Bocanegra, D. Davidenko, V. Sarou-Kanian, C. Chauveau, I. Gökalp, Experimental and numerical studies on the burning of aluminum micro and nanoparticle clouds in air, *Exp. Thermal Fluid Sci.* 34 (2010) 299–307, <http://dx.doi.org/10.1016/j.expthermflusci.2009.10.009>.
- [10] R. Khatami, Y.A. Leventdis, An overview of coal rank influence on ignition and combustion phenomena at the particle level, *Combust. Flame* 164 (2016) 22–34, <http://dx.doi.org/10.1016/j.combustflame.2015.10.031>.
- [11] G. Simões, D. Magalhães, M. Rabaçal, M. Costa, Effect of gas temperature and oxygen concentration on single particle ignition behavior of biomass fuels, in: *Proceedings of the Combustion Institute*. <http://dx.doi.org/10.1016/j.proci.2016.06.102>.
- [12] G. Wang, R.B. Silva, J.L.T. Azevedo, S. Martins-Dias, M. Costa, Evaluation of the combustion behaviour and ash characteristics of biomass waste derived fuels, pine and coal in a drop tube furnace, *Fuel* 117 (Part A) (2014) 809–824, <http://dx.doi.org/10.1016/j.fuel.2013.09.080>.
- [13] F.F. Costa, G. Wang, M. Costa, Combustion kinetics and particle fragmentation of raw and torrefied pine shells and olive stones in a drop tube furnace, *Proc. Combust. Inst.* 35 (2015) 3591–3599, <http://dx.doi.org/10.1016/j.proci.2014.06.024>.
- [14] S. Pereira, P.C.R. Martins, M. Costa, Kinetics of poplar short rotation coppice obtained from thermogravimetric and drop tube furnace experiments, *Energy Fuels* 30 (2016) 6525–6536, <http://dx.doi.org/10.1021/acs.energyfuels.6b01313>.
- [15] C.R. Shaddix, A. Molina, Particle imaging of ignition and devolatilization of pulverized coal during oxy-fuel combustion, *Proc. Combust. Inst.* 32 (2009) 2091–2098, <http://dx.doi.org/10.1016/j.proci.2008.06.157>.
- [16] R.G. Kim, D. Li, C.H. Jeon, Experimental investigation of ignition behavior for coal rank using a flat flame burner at a high heating rate, *Exp. Thermal Fluid Sci.* 54 (2014) 212–218, <http://dx.doi.org/10.1016/j.expthermflusci.2013.12.017>.
- [17] R. Khatami, C. Stivers, K. Joshi, Y.A. Leventdis, A.F. Sarofim, Combustion behavior of single particles from three different coal ranks and from sugar cane bagasse in O_2/N_2 and O_2/CO_2 atmospheres, *Combust. Flame* 159 (2012) 1253–1271, <http://dx.doi.org/10.1016/j.combustflame.2011.09.009>.
- [18] J. Köser, L. Becker, N. Vorobiev, M. Schiemann, V. Scherer, B. Böhm, A. Dreizler, Characterization of single coal particle combustion within oxygen-enriched environments using high-speed OH-PLIF, *Appl. Phys. B* 121 (2015) 459–464, <http://dx.doi.org/10.1007/s00340-015-6253-3>.
- [19] F. Podczeczek, A shape factor to assess the shape of particles using image analysis, *Powder Technol.* 93 (1997) 47–53, [http://dx.doi.org/10.1016/S0032-5910\(97\)03257-9](http://dx.doi.org/10.1016/S0032-5910(97)03257-9).
- [20] L. Gao, Y. Yan, G. Lu, R.M. Carter, On-line measurement of particle size and shape distributions of pneumatically conveyed particles through multi-wavelength based digital imaging, *Flow Meas. Instrum.* 27 (2012) 20–28, <http://dx.doi.org/10.1016/j.flowmeasinst.2012.03.011>.
- [21] R.M. Carter, Y. Yan, S.D. Cameron, On-line measurement of particle size distribution and mass flow rate of particles in a pneumatic suspension using combined imaging and electrostatic sensors, *Flow Meas. Instrum.* 16 (2005) 309–314, <http://dx.doi.org/10.1016/j.flowmeasinst.2005.03.005>.
- [22] X. Qian, Y. Yan, L. Wang, J. Shao, An integrated multi-channel electrostatic sensing and digital imaging system for the on-line measurement of biomass-coal particles in fuel injection pipelines, *Fuel* 151 (2015) 2–10, <http://dx.doi.org/10.1016/j.fuel.2014.11.013>.
- [23] S. Ouyang, H. Yeasmin, J. Mathews, A pressurized drop-tube furnace for coal reactivity studies, *Rev. Sci. Instrum.* 69 (1998) 3036–3041, <http://dx.doi.org/10.1063/1.1149052>.
- [24] A.C. Sarroza, T.D. Bennet, C. Eastwick, H. Liu, Characterising pulverised fuel ignition in a visual drop tube furnace by use of a high-speed imaging technique, *Fuel Process. Technol.* 157 (2017) 1–11, <http://dx.doi.org/10.1016/j.fuproc.2016.11.002>.
- [25] X. Bai, G. Lu, T. Bennet, Y. Peng, H. Liu, C. Eastwick, Y. Yan, Measurement of coal particle combustion behaviors in a drop tube furnace through high-speed imaging and image processing, in: Presented at the IEEE International

- Instrumentation and Measurement Technology Conference, Taipei, Taiwan, 23–26 May 2016, <http://dx.doi.org/10.1109/I2MTC.2016.7520582>.
- [26] N. Otsu, A threshold selection method from gray-level histograms, *Automatica* 11 (1975) 23–27.
- [27] C.W. Nan, R. Birringer, D.R. Clarke, H. Gleiter, Effective thermal conductivity of particulate composites with interfacial thermal resistance, *J. Appl. Phys.* 81 (1997) 6692–6699, <http://dx.doi.org/10.1063/1.365209>.
- [28] I. Kunttu, L. Lepistö, Shape-based retrieval of industrial surface defects using angular radius Fourier descriptor, *IET Image Proc.* 1 (2007) 231–236, <http://dx.doi.org/10.1049/iet-ipr:20060113>.
- [29] D. Zhang, G. Lu, Study and evaluation of different Fourier methods for image retrieval, *Image Vis. Comput.* 23 (2005) 33–49, <http://dx.doi.org/10.1016/j.imavis.2004.09.001>.
- [30] X. Wu, Q. Wang, Z. Luo, M. Fang, K. Cen, Experimental study of particle rotation characteristics with high-speed digital imaging system, *Powder Technol.* 181 (2008) 21–30, <http://dx.doi.org/10.1016/j.powtec.2007.04.007>.
- [31] R.M. Haralick, L.G. Shapiro, *Computer and Robot Vision*, Vol. 1, Addison-Wesley, US, 1992, pp. 639–658.